Probing Microplasticity in Small-Scale FCC Crystals via Dynamic Mechanical Analysis

Xiaoyue Ni,[1,*] Stefanos Papanikolaou,[2,3,4] Gabriele Vajente,[5] Rana X Adhikari,[5] and Julia R. Greer[1]
[1]Division of Engineering and Applied Sciences, California Institute of Technology, Pasadena, California 91125, USA
[2]Department of Mechanical Engineering, Johns Hopkins University, 3400 N Charles St, Baltimore, Maryland 21218, USA
[3]Department of Mechanical and Aerospace Engineering, West Virginia University, 395 Evansdale Dr, Morgantown, West Virginia 26506, USA
[4]Department of Physics, West Virginia University, 135 Willey St, Morgantown, West Virginia 26506, USA
[5]LIGO Laboratory, California Institute of Technology, Pasadena, California 91125, USA
(Received 23 December 2016; published 14 April 2017)

In small-scale metallic systems, collective dislocation activity has been correlated with size effects in strength and with a steplike plastic response under uniaxial compression and tension. Yielding and plastic flow in these samples is often accompanied by the emergence of multiple dislocation avalanches. Dislocations might be active preyield, but their activity typically cannot be discerned because of the inherent instrumental noise in detecting equipment. We apply alternate current load perturbations via dynamic mechanical analysis during quasistatic uniaxial compression experiments on single crystalline Cu nanopillars with diameters of 500 nm and compute dynamic moduli at frequencies 0.1, 0.3, 1, and 10 Hz under progressively higher static loads until yielding. By tracking the collective aspects of the oscillatory stress-strain-time series in multiple samples, we observe an evolving dissipative component of the dislocation network response that signifies the transition from elastic behavior to dislocation avalanches in the globally preyield regime. We postulate that microplasticity, which is associated with the combination of dislocation avalanches and slow viscoplastic relaxations, is the cause of the dependency of dynamic modulus on the driving rate and the quasistatic stress. We construct a continuum mesoscopic dislocation dynamics model to compute the frequency response of stress over strain and obtain a consistent agreement with experimental observations. The results of our experiments and simulations present a pathway to discern and quantify correlated dislocation activity in the preyield regime of deforming crystals.

DOI: 10.1103/PhysRevLett.118.155501

Introduction.—Mechanical deformation of materials is usually described by continuous, deterministic stress-strain relations; for examples, see Ref. [1]. In the last decade, Uchic *et al.* first applied the uniaxial compression methodology on focused ion beam (FIB)-machined Ni micropillars [2]. Greer and Nix then extended it to Au nanopillars [3], and since then the discrete and stochastic deformation of small-scale single-crystalline metals has been ubiquitously observed, with smaller pillars exhibiting higher yield stresses [4–7]. The large strain bursts are unambiguously distinguished as serrations in the stress-strain curves as shown in Fig. 1(a). They have been mainly attributed to the unique nanoscale plasticity mechanisms, where the operation of individual dislocation sources, single arm or surface, governs deformation and strength [8,9]. The extent of these strain bursts usually ranges from nanometers to a few microns [2,4,10,11]. The analysis of strain bursts shows that the slip size distributions follow power laws [4,12], with system-size- [13,14] and stress- [10,15] dependent cutoffs. It is unclear whether smaller strain bursts, undetected by the instrument, are present in the deformation of such micro- and nanosized single crystals, especially prior to the yield point, commonly defined as the start of the first detected burst, as shown in Fig. 1(a) at stress σ_{ys}. While small, these events compose mechanical noise that is imperative to understand and remove for high-precision experiments, such as the Advanced Laser Interferometer Gravitational-Wave Observatory (LIGO) [16,17]—the impulsive strain events propagated from the metallic suspension system to the test mass [18] can introduce background noise which could limit the interferometer sensitivity.

Using basic forms of mechanical loading, such as a force- or displacement-controlled compression, careful examination of the data provided evidence for the presence of short plastic instabilities before the onset of the obvious and apparent strain bursts [10,19–21], e.g., 100–400 MPa regime of 500 nm pillars, as shown in Fig. 1(a). The higher yield stress observed in small-scale samples compared to their macroscopic counterparts can be understood in terms of dislocation starvation, where upon compression, the initially present mobile dislocations have a higher probability of annihilating at a nearby free surface than multiplying or being entangled with other dislocations [22,23]. This dislocation source exhaustion mechanism might involve preyield dislocation activities. *In situ* transmission electron microscope (TEM) nanoindentation experiments revealed the onset of dislocation motion before the first obvious displacement excursion [24,25]. *In situ* Laue microdiffraction work with micron-sized Ni sample

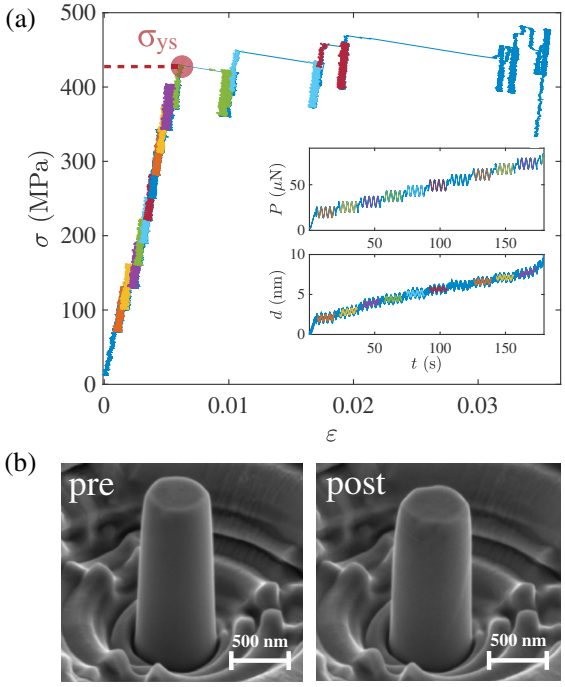

FIG. 1. *Dynamic mechanical analysis on Cu nanopillars.* (a) Engineering stress vs strain during DMA measurements on a Cu sample at a frequency of 0.3 Hz; different colors separate data taken at different steps of stress-oscillation segments. The inset shows raw load vs displacement as a function of time in the preyield regime. The overlaying different color curves are sinusoidal fits for each data set of oscillation segments, using Eqs. (1a) and (1b). (b) SEM images of an as-fabricated (pre-) and compressed (post-) ~500 nm diameter Cu pillar with a nominal aspect ratio of 3:1.

showed that a dislocation structure forms at ~0.65 of the yield stress and continues to develop until global yielding is reached [26]. Creep experiments on single crystals of ice detected acoustic emission events at resolved shear stresses far below the yield stress [27]. These observations have yet to be connected to constitutive relations and a quantifiable stress-strain response. Discrete dislocation dynamics (DDD) simulations suggest the existence of intermittent events in the preyield regime of crystalline materials [28,29] and a significant loading rate effect on strain burst response of nano- and microcrystals due to dislocation jamming and relaxation [30]. Stress-induced probabilistic cross-slip relaxation has also been associated with several nontrivial aspects of crystal plasticity [31]. It is natural to question whether we can detect and quantify microplasticity in crystals' preyield regime.

Machine noise has been the Achilles' heel of numerous experimental nanomechanical investigations. Attempts have been made to characterize the machine noise, with reported values of ~0.2 nm displacement-, ~30 nN force- noise floor, and a thermal drift of < 0.05 nm/s for the prevalently used Hysitron TI 950 Triboindenter in quasistatic mode [32]. In uniaxial compression experiments, a flat nanoindenter tip applies compressive load to the top of a commonly cylindrical sample, a so-called micro- or nanopillar, and the indenter-sample friction, as well as the electromagnetic assembly responsible for the load control produce substantial and inevitable machine noise. In addition, noise caused by thermal drift sets a limit on the duration of such experiments, which renders long-time mechanical experiments like cyclical or fatigue loading, as well as creep tests, virtually impossible to interpret. Statistical probing is necessary to detect any possible nonlinear dislocation activities, which cause axial displacements below the machine noise. We apply dynamic mechanical analysis (DMA) at multiple frequencies that span three orders of magnitude, from 0.1 to 10 Hz, on multiple 500 nm-diameter single crystalline Cu nanopillars. We statistically characterize the overall DMA behavior and compare it with mean-field dislocation depinning predictions.

Experiment.—Cylindrical nanopillars with diameters of ~500 nm and aspect ratios (height/diameter) of ~3:1 were fabricated following a concentric-circles top-down methodology using a focused ion beam [14,33,34] from bulk single-crystalline copper (>99.9999% purity) with one side polished to a <30 Å rms roughness, oriented in ~$\langle 111 \rangle$ direction [35]. Although FIB introduces surface damage to the pillars by forming small dislocation loops or an amorphous layer [36], it is the initial microstructure rather than the fabrication technique that determines the deformation mechanism of small-scale fcc metals [19]. The nanomechanical experiments were carried out in a nanoindenter (Triboindenter, Hysitron [32]) equipped with an 8 μm-diameter flat punch diamond tip custom made specifically for these experiments. Figure 1(a) conveys a representative compressive engineering stress-strain data, with the inset showing the corresponding time series of load and displacement, zoomed into the preyield regime. In the experiment, we applied a uniaxial quasistatic load that monotonically increased in a stepwise fashion to an individual nanopillar. Small stress oscillations with the amplitude of 6 μN and a fixed frequency in the range between 0.1 and 10 Hz were superimposed over the static load to each 15-s step interval. Before the initiation of each compression experiment, we waited for >145 s to equilibrate the in-contact displacement drift and used the last 20-s drift data to estimate the thermal drift rate for subsequent correction. Only those experiments where the thermal drift rate was less than 0.05 nm/s were analyzed. The loading time before the occurrence of the first large strain event was usually within the first 200 s for all tests. Figure 1(b) shows the representative pre- and post-compression SEM images of a representative Cu nanopillar.

The dynamic modulus is defined as the frequency response of stress over strain $E(\omega, \sigma_0) = \sigma(\omega)/\varepsilon(\omega)$, where σ_0 is the applied quasistatic stress and $\omega = 2\pi f$ is the driving frequency. Using this definition, we can extract the dynamic modulus from the oscillations that are imposed at each quasistatic stress σ_0 using a frequency domain analysis.

We fit the time series of stress $\sigma(t)$ and strain $\varepsilon(t)$ using the following form which also includes a linear drift term:

$$\sigma_f(t) = x_r \cos(\omega t) + x_i \sin(\omega t) + \sigma_d t + \sigma_0, \quad (1a)$$

$$\varepsilon_f(t) = u_r \cos(\omega t) + u_i \sin(\omega t) + \varepsilon_d t + \varepsilon_0, \quad (1b)$$

where $x_r, x_i, \sigma_d, \sigma_0, u_r, u_i, \varepsilon_d, \varepsilon_0$ are fitting parameters for the stress and strain. The complex dynamic modulus E can then be calculated as a function of the ω and σ_0,

$$E(\omega, \sigma_0) = \frac{x_r - i x_i}{u_r - i u_i} = A(\omega, \sigma_0) e^{i\phi(\omega, \sigma_0)}, \quad (2)$$

where A and ϕ are the amplitude and phase components of the dynamic modulus.

We applied this type of DMA using different driving frequencies: 0.1, 0.3, 1, and 10 Hz, for each quasistatic load hold and took measurements from six samples for each frequency driving test. We solved for the dynamic modulus at each quasistatic loading step at the single driving frequency using the fitting procedure described above. The quasistatic stress at each step is normalized by the yield stress of the system σ_{ys}. We binned amplitude and phase lag for sample statistics. The binning mean and standard error for amplitude and phase lag were calculated as a function of the stress bin centers and are shown for each driving frequency in Fig. 2(a). The DMA data reveal a maximum of ~70% decrease in the average amplitude and a maximum of ~60° increase in the average phase lag as the applied quasistatic stress approaches yielding at $\sigma_0/\sigma_{ys} = 1$ (~400 MPa). This plot also shows that these deviations from elastic behavior are more pronounced for slower driving frequencies. These results are in stark contrast to the DMA data collected from the same type of uniaxial compression on a ~500 nm-diameter fused silica nanopillars, which exhibits a constant amplitude of ~65 GPa and a no-delay response for the driving frequencies of 1 Hz and 10 Hz.

Simulation.—To reveal the underlying mechanisms that drive the observed nontrivial loss behavior in Cu as the applied stress approaches yielding, we constructed a continuum crystal plasticity model that aims at capturing the salient aspects of the observed mechanical behavior. This model considers the energetics of two competing processes: the dislocation-driven abrupt strain jumps and the slow stress-controlled relaxations towards minimum system energy state. To capture both the fast avalanches and the slow viscoplastic relaxations, we utilized a cellular automaton constitutive microplasticity model enhanced with an additional continuous-in-time strain field that follows a viscoplastic constitutive law [31,37,38]. We model the shear strain to consist of the elastic and plastic components $\gamma = \gamma_e + \gamma_p$. The elastic term is calculated using Hooke's law. The plasticity model that captures the plastic term can be realized using detailed continuum plasticity modeling approaches [1]. It is reasonable to assume that in a single representative volume element

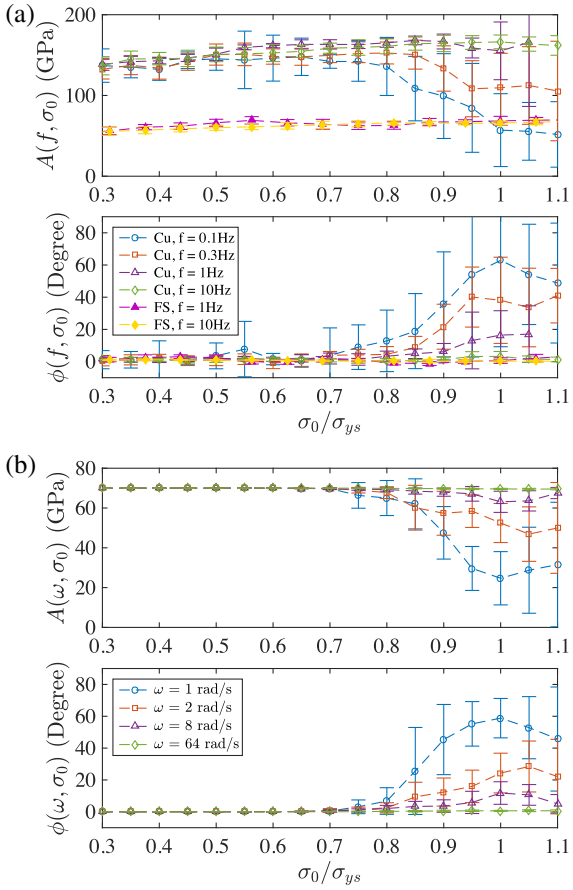

FIG. 2. *Dynamic modulus vs stress.* (a) The experimental DMA results on copper and fused silica (FS) 500 nm pillars. The amplitude A and phase ϕ of the dynamic modulus values are statistically analyzed from six samples for driving varying from 0.1 Hz to 10 Hz, both plotted versus the global stress, around which the oscillations were applied. This plot demonstrates that the dynamic modulus is not constant as the quasistatic load approaches the yield point, and the deviation gets larger with slower driving. (b) DMA results from the mesoscopic dislocation dynamics simulation.

for single-crystalline fcc crystals, the following criteria hold: (i) uniaxial loading activates one dominant crystallographic slip system, A, with another system, B, assisting dislocation glide along A [39] and (ii) dislocations carry plastic distortion via two distinct mechanisms: (a) fast dislocation avalanchelike glide and (b) slow, stress-relaxation-driven secondary glide on A caused by the coupled A-B dislocation mechanisms (e.g., double cross slip) [31]. With contributions from both mechanisms, the total plastic strain can be expressed as

$$\gamma_p = \gamma_p^{(a)} + \gamma_p^{(b)}. \quad (3)$$

In the fast dislocation avalanche-driven mechanism, a volume element at location $\mathbf{r}$ yields a random plastic strain $\delta\gamma_p^{(a)}$ if the local stress $\tau(\mathbf{r})$ is larger than a local depinning threshold $\chi(\mathbf{r})$ [31,40,41], where $\chi(\mathbf{r})$ follows a uniform

distribution [42]. After each avalanche, the threshold value is redrawn from the same distribution. On the other hand, the slow relaxation mechanism follows a typical constitutive viscoplastic law,

$$\dot{\gamma}_p^{(b)} = \frac{D}{G}(\tau(\mathbf{r}))^n, \tag{4}$$

where D is the relaxation constant, G is the shear modulus, and $n \in [1, 3] < 10$ is the critical quantity to define another time scale which is slow compared to the fast avalanche process [20].

For numerical simplicity, we apply this methodology to edge dislocations only, for which the local resolved shear stress can be explicitly calculated

$$\tau(\mathbf{r}) = \tau_{\text{ext}} + \tau_{\text{int}}(\mathbf{r}) + \tau_{\text{hard}}(\mathbf{r}) = \tau_0 + \tau_A \sin(\omega t) + \int d^2\mathbf{r}' K(\mathbf{r} - \mathbf{r}')\gamma_p(\mathbf{r}') - h\gamma_p(\mathbf{r}), \tag{5}$$

where τ_{ext} is the applied external quasistatic stress combined with the oscillation component, τ_{int} is the stress that accounts for the long-range interactions with other dislocations, and τ_{hard} is the stress that arises from dislocation hardening. In the expanded form of Eq. (5), K serves as the interaction kernel for single slip straight edge dislocations, and h represents a mean-field phenomenological hardening parameter [37,38]. For the stress kernels of complete circular dislocation loops or screws, in principle, the results would be unchanged, since all these kernels are sufficiently long ranged [40,47]. The model implementation is such that the system is meshed into $N \times N$ elements, with $N = 32$. We prescribe similar loading conditions to eight random initial configurations as we did in the experiments, with different driving frequencies of 1, 2, 8, and 64 rad/s. The rate equation associated to Eq. (3) can be numerically solved by Euler integration with a fixed time step $\Delta t = 10^{-2}$ s. Additional simulation details are provided in Supplemental Materials [42].

Discussion.—Figure 2(b) shows the same frequency domain analysis of the dynamic modulus using simulations results as the ones shown in Fig. 2(a) for the experimental data. This qualitative agreement between simulations and experiments motivates a further quantitative comparison. Existing simulations investigated the effect of cyclic loading on the evolved dislocation network and predicted a scaling relation between the normalized strain rate amplitude and the driving frequency, focused on the mean-field depinning theory framework [28,48],

$$\frac{|\dot{\varepsilon}|}{|\sigma|} \sim \omega^{\kappa}, \tag{6}$$

where $\kappa = 1$ corresponds to a simple harmonic oscillator, i.e., perfectly elastic behavior, and $\kappa = 0.82$ corresponds to a system driven close to the pinning threshold F. The strain rate amplitude is normalized by the stress amplitude, $|\dot{\varepsilon}|/|\sigma|$ which is equivalent to ω/A, where A is the dynamic modulus amplitude measured via DMA. Figure 3 shows

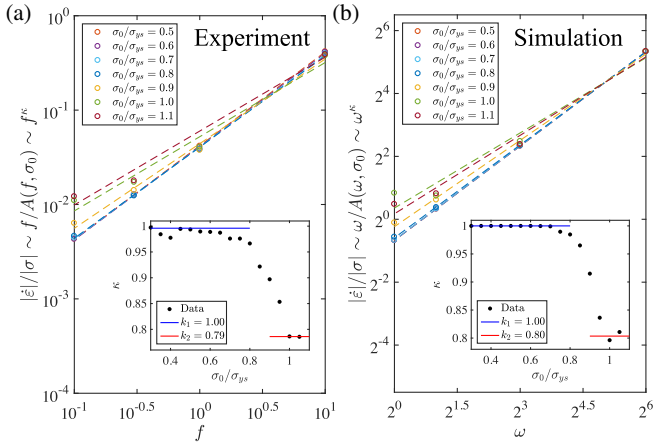

FIG. 3. *Scaling analysis of the normalized strain-rate amplitude.* (a) The normalized strain rate amplitude scaling over driving frequency analysis [28] using experimental DMA data and (b) simulation DMA data. The figures show explicitly the fitting for scaling parameter κ using Eq. (6) at different quasistatic stress levels. The inset presents the measured κ as a function of normalized stress.

the scaling analysis of the normalized strain rate amplitude vs driving frequency for the dynamic modulus amplitude calculated from the experiments and simulations at different quasistatic loads. The insets show the scaling parameter κ as a function of the normalized stress. These plots convey that at both small and large stress regimes, experiments and simulations produce scaling behaviors that are in agreement with the mean-field depinning predictions, and a smooth, microplastic crossover connects these two extreme regimes. The experiments and simulations reveal enhanced microplasticity activities as the system is stressed close to yielding. The actual mechanism that is responsible for the increased "susceptibility" to plasticity can be a thermally activation process like cross slip, or the collective dislocation bowing out due to long-range interactions, i.e., the Andrade mechanism [49].

Summary.—We imposed oscillatory loads in the nominal elastic regime of the uniaxially compressed 500 nm-diameter single crystalline Cu nanopillars. We applied monotonically increasing stresses above the bulk yield point of ~10 MPa [50,51] to investigate the mechanically correlated material response. Analysis of the cumulative oscillatory response reveals a substantial deviation from the nominally perfectly elastic behavior, as well as an emergent dissipation signature in what has always been considered preyield regime. This finding resembles prior research on amplitude-dependent internal friction in metallic materials [52,53]. Our experimental observations are corroborated by a mesoscale dislocation plasticity model, which accounts for dislocation avalanches (fast processes) and the viscoplastic response (slow time scales) during oscillatory loading. We formulate a scaling analysis that shows a smooth transition of the system from perfect elasticity to dislocation

depinning-driven plasticity that occurs at loads lower than the global yield stress. This approach represents a new pathway to investigate and quantify the abrupt plastic events that emanate from dislocation activities even in the preyield regime, that occur ubiquitously during deformation of small-scale single crystals below instrumental noise levels.

The developed methodology can be applied to characterize preyield dislocation dynamics in extensive list of fcc, bcc, and hcp materials. The micromechanical study sheds light on detecting crackling noise in macroscopic sample subjected to nominal elastic loading. The observation of such events might lead to better prediction of plastic yielding and even incipient fracture for structural materials. The preyield mechanical noise itself can be a hidden problem for instrumentation that requires high strain sensitivity, e.g., advanced LIGO [16,17].

We would like to thank Eric K. Gustafson, Koji Arai, Eric Quintero, and the members of the Seismic Isolation and Suspension Working Group in the LIGO Scientific Collaboration, as well as Peter Ispanovity and Erik Van der Giessen for helpful discussions. We thank Ottman Turtuliano for assistance with fused silica sample preparation. We gratefully acknowledge the financial support from NSF (DMR-1204864, JRG) and the Department of Energy, Basic Energy Sciences [Early Career Faculty grant (JRG) and DE-SC0014109 (SP)]. LIGO was constructed by the California Institute of Technology and Massachusetts Institute of Technology using funding from the National Science Foundation, and operates under Cooperative Agreement No. PHY-0757058. Advanced LIGO was built under Award No. PHY-0823459. This paper carries LIGO Document No. LIGO-P1600316.

*Corresponding author.
xnni@caltech.edu

[1] R. Asaro and V. Lubarda, *Mechanics of Solids and Materials* (Cambridge University Press, Cambridge, England, 2006).
[2] M. D. Uchic, D. M. Dimiduk, J. N. Florando, and W. D. Nix, Science **305**, 986 (2004).
[3] J. R. Greer, W. C. Oliver, and W. D. Nix, Acta Mater. **53**, 1821 (2005).
[4] D. M. Dimiduk, C. Woodward, R. LeSar, and M. D. Uchic, Science **312**, 1188 (2006).
[5] M. D. Uchic, P. A. Shade, and D. M. Dimiduk, Annu. Rev. Mater. Res. **39**, 361 (2009).
[6] O. Kraft, P. A. Gruber, R. Monig, and D. Weygand, Annu. Rev. Mater. Res. **40**, 293 (2010).
[7] J. R. Greer and J. Th. M. De Hosson, Prog. Mater. Sci. **56**, 654 (2011).
[8] S. I. Rao, D. M. Dimiduk, M. Tang, M. D. Uchic, T. A. Parthasarathy, and C. Woodward, Philos. Mag. **87**, 4777 (2007).
[9] T. A. Parthasarathy, S. I. Rao, D. M. Dimiduk, M. D. Uchic, and D. R. Trinkle, Scr. Mater. **56**, 313 (2007).
[10] N. Friedman, A. T. Jennings, G. Tsekenis, J.-Y. Kim, M. Tao, J. T. Uhl, J. R. Greer, and K. A. Dahmen, Phys. Rev. Lett. **109**, 095507 (2012).
[11] R. Maaß, P. M. Derlet, and J. R. Greer, Scr. Mater. **69**, 586 (2013).
[12] J. P. Sethna, K. A. Dahmen, and C. R. Myers, Nature (London) **410**, 242 (2001).
[13] F. F. Csikor, C. Motz, D. Weygand, M. Zaiser, and S. Zapperi, Science **318**, 251 (2007).
[14] S. Brinckmann, J.-Y. Kim, and J. R. Greer, Phys. Rev. Lett. **100**, 155502 (2008).
[15] K. A. Dahmen, Y. Ben-Zion, and J. T. Uhl, Phys. Rev. Lett. **102**, 175501 (2009).
[16] J. Aasi *et al.*, Classical Quantum Gravity **32**, 074001 (2015).
[17] G. Vajente, E. A. Quintero, X. Ni, K. Arai, E. K. Gustafson, N. A. Robertson, E. J. Sanchez, J. R. Greer, and R. X. Adhikari, Rev. Sci. Instrum. **87**, 065107 (2016).
[18] S. M. Aston *et al.*, Classical Quantum Gravity **29**, 235004 (2012).
[19] A. T. Jennings, M. J. Burek, and J. R. Greer, Phys. Rev. Lett. **104**, 135503 (2010).
[20] A. T. Jennings, J. Li, and J. R. Greer, Acta Mater. **59**, 5627 (2011).
[21] R. Maaß, M. Wraith, J. T. Uhl, J. R. Greer, and K. A. Dahmen, Phys. Rev. E **91**, 042403 (2015).
[22] D. M. Dimiduk, M. D. Uchic, and T. A. Parthasarathy, Acta Mater. **53**, 4065 (2005).
[23] J. R. Greer and W. D. Nix, Phys. Rev. B **73**, 245410 (2006).
[24] A. M. Minor, S. A. Syed Asif, Z. W. Shan, E. A. Stach, E. Cyrankowski, T. J. Wyrobek, and Oden L. Warren, Nat. Mater. **5**, 697 (2006).
[25] Z. W. Shan, R. K. Mishra, S. A. Syed Asif, Oden L. Warren, and A. M. Minor, Nat. Mater. **7**, 115 (2008).
[26] R. Maaß and and M. D Uchic, Acta Mater. **60**, 1027 (2012).
[27] M.-Carmen Miguel, A. Vespignani, S. Zapperi, J. Weiss, and J.-R. Grasso, Nature (London) **410**, 667 (2001).
[28] L. Laurson and M. J. Alava, Phys. Rev. Lett. **109**, 155504 (2012).
[29] P. D. Ispánovity, L. Laurson, M. Zaiser, I. Groma, S. Zapperi, and M. J. Alava, Phys. Rev. Lett. **112**, 235501 (2014).
[30] Y. Cui, G. Po, and N. Ghoniem, Phys. Rev. Lett. **117**, 155502 (2016).
[31] S. Papanikolaou, D. M. Dimiduk, W. Choi, J. P. Sethna, M. D. Uchic, C. F. Woodward, and S. Zapperi, Nature (London) **490**, 517 (2012).
[32] Hysitron TI 950 Triboindenter, https://www.hysitron.com, accessed July 20, 2016.
[33] J.-Y. Kim and J. R. Greer, Acta Mater. **57**, 5245 (2009).
[34] J.-Y. Kim, D. Jang, and J. R. Greer, Acta Mater. **58**, 2355 (2010).
[35] MTI corp., http://www.mtixtl.com/, accessed July 20, 2016.
[36] D. Kiener, C. Motz, M. Rester, M. Jenko, and G. Dehm, Mater. Sci. Eng. A **459**, 262 (2007).
[37] M. Zaiser and P. Moretti, J. Stat. Mech. (2005) P08004.
[38] M. Zaiser, Adv. Phys. **55**, 185 (2006).
[39] Although the bulk is nominally high-symmetry orientated, in a large deformation picture, the pillars would point towards dominant slip systems. The $\sim\langle 111\rangle$ orientation leads to a slip system with near zero resolved shear stress, leaving lots of dislocations that can function as the B slip system [19].

[40] D. S. Fisher, Phys. Rep. **301**, 113 (1998).
[41] W. H. Press, S. A. Teukolsky, W. T. Vetterling, and B. P. Flannery, *Numerical Recipes in C: The Art of Scientific Computing* (Cambridge University Press, Cambridge, England, 1988).
[42] See Supplemental Material at http://link.aps.org/supplemental/10.1103/PhysRevLett.118.155501, which includes Refs. [43–46].
[43] J. Bonneville, B. Escaig, and J. L. Martin, Acta Metall. **36**, 1989 (1988).
[44] S. I. Rao, D. M. Dimiduk, J. A. El-Awady, T. A. Parthasarathy, M. D. Uchic, and C. Woodward, Acta Mater. **58**, 5547 (2010).
[45] J. R. Davis and ASM International Handbook Committee, *Copper and Copper Alloys* (ASM International, Materials Park, 2001), p. 451.
[46] M. Talamali, V. Petäjä, D. Vandembroucq, and S. Roux, Phys. Rev. E **84**, 016115 (2011).
[47] N. M. Ghoniem, J. Huang, and Z. Wang, Philos. Mag. Lett. **82**, 55 (2002).
[48] F. Schütze and T. Nattermann, Phys. Rev. B **83**, 024412 (2011).
[49] M.-Carmen Miguel, A. Vespignani, M. Zaiser, and S. Zapperi, Phys. Rev. Lett. **89**, 165501 (2002).
[50] H. Mughrabi, Mater. Sci. Eng. **33**, 207 (1978).
[51] P. Ambrosi, E. Göttler, and Ch. Schwink, Scr. Metall. **8**, 1093 (1974).
[52] F. R. N. Nabarro, *Theory of Crystal Dislocations* (Clarendon Press, Oxford, 1967).
[53] M. S. Blanter, I. S. Golovin, H. Neuhäuser, and H.-R. Sinning, *Internal Friction in Metallic Materials: A Handbook* (Springer, Berlin, 2007).